ELSEVIER

Journal of Nuclear Materials 266–269 (1999) 513–519

journal of nuclear materials

Carbon and neon penetration near a neutraliser plate of the Tore Supra ergodic divertor

R. Guirlet [a,*], J. Hogan [b], L. Chérigier [c], C. DeMichelis [a], P. Ghendrih [a], A. Grosman [a], D. Guilhem [a], B. Meslin [a], P. Monier-Garbet [a]

[a] *Assoc. EURATOM-CEA sur la Fusion, C.E. Cadarache, 13108 St-Paul-lez-Durance, France*
[b] *Oak Ridge National Laboratory, Fusion Energy Division, PO Box 2009, Oak Ridge, TN 37831-8072, USA*
[c] *PIIM, Case 321, Faculté des Sciences St-Jérôme, Avenue Normandie-Niémen, 13397 Marseille, France*

Abstract

The ergodic divertor (ED) of Tore Supra has been shown to diminish core impurity contamination. To assess this effect on injected neon a scan in ED perturbation intensity is reported. Spectroscopic observations of neon on an ED neutraliser plate (NP) show that the penetration of low neon ionisation stages increases with the perturbation intensity while the ratio of the edge to central neon density increases. A scan in volume average density is also reported, showing that, at maximum ED perturbation, the carbon penetration decreases with increasing densities up to values close to detachment. Modelling of these experiments with the 2D code IMPEN and the 3D code BBQ shows the importance of a realistic description of the neutral source and of n_e and T_e in the vicinity of the NP.

Keywords: Ergodic divertor; Impurity screening; Penetration; Plasma edge; Spectroscopy

1. Introduction

Highly radiating regimes in tokamaks are considered to be a solution to the excessive heat load on the plasma facing components of next generation devices. The Tore Supra (TS) ergodic divertor, made of six octopolar coils equally spaced toroidally, has proved to be an efficient tool to achieve such regimes [1,2]. The perturbed magnetic field topology characteristic of the ergodic divertor (ED) configuration leads to a low confinement region at the plasma edge, of radial extension of the order of 7 cm at maximum ED current ($I_{ED} = 45$ kA). This region is dominated by parallel transport. Due to the deflection of the perturbed field lines towards the wall in the vicinity of the ED coils, a high recycling regime with high edge densities may be induced [3]. The neutrals produced there are more likely to be ionised and to radiate without entering the confined plasma. The ED has been designed such that most of these plasma–wall interactions take place on the ED neutraliser plates (NPs). This 'screening effect' (also observed in Refs. [4,5]) allows to maintain a relatively high edge impurity concentration compared to the bulk one. ED experiments have shown that this screening effect depends on the considered species [6] as well as on the electron density and temperature in the plasma edge. Two essential quantities in the ED effect are studied here: the radial depth of the perturbed region, depending on the magnetic perturbation intensity, and the ionisation length, depending on the density regime. This paper is organised as follows. Section 2 is dedicated to the presentation of the TS diagnostics of interest for the present study. In Section 3, we report an experimental study of the radial depth of the perturbed region, in which the first two ionisation stages of Ne were observed. In Section 4 we discuss the carbon ions line brightness during a density scan experiment in the upper range of densities used in TS. Section 5 is dedicated to the 2D code IMPEN and the 3D code BBQ used to interpret the experiments.

* Corresponding author. Tel.: +33-4 42 25 38 85; fax: +33-4 42 25 62 33; e-mail: guirlet@drfc.cad.cea.fr

0022-3115/99/$ – see front matter
PII: S0022-3115(98)00831-9

2. Diagnostics

All the results presented here concern the midplane ED neutraliser plate located on one of the six ED modules (Fig. 1). The plate is actually made of four copper needles coated with B_4C, the vents between needles being connected to a titanium pump. The visible spectroscopic observation in front of the NP uses four in situ optical fibres equipped with small telescopes. The four fibres are connected to a high resolution Czerny–Turner spectrometer equipped with a 1200 g/mm grating and a CCD camera (400–1100 nm), allowing to observe 4–7 nm wide spectra. The four lines of sight are close to parallel to the NP plane (6.2° at maximum), with an opening half angle of about 2°, covering the region within 8 cm radially away from the plate.

The NP is equipped with a Langmuir probe located 3 cm from its tip. In order to get some information about the n_e and T_e profiles along the NP, we also use three Langmuir probes located at different positions along the corresponding NP of the neighbouring module, assuming the $2\pi/6$ toroidal periodicity induced by the ED geometry. As long as the plasma is attached to the NP, no significant difference in n_e is observed between the various probes. Therefore a flat n_e profile along the NP will be assumed in the following. As far as T_e is concerned, the infra-red thermographic measurements of the heat flux ($\propto T_e^{5/2}$) deposited on the NP, consistent with the Langmuir probe data but with a better spatial resolution, show a structure. However, the height (a factor 1.5 above the average) and width (about 4 cm) of this T_e structure are small. Therefore they are assumed not to influence the general trends in the impurity ion behaviour. In the 2D model, a flat T_e profile deduced from the Langmuir probes will be assumed. In the 3D code BBQ this structure is taken into account.

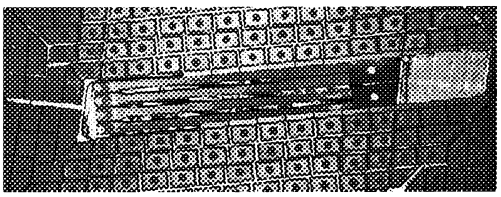

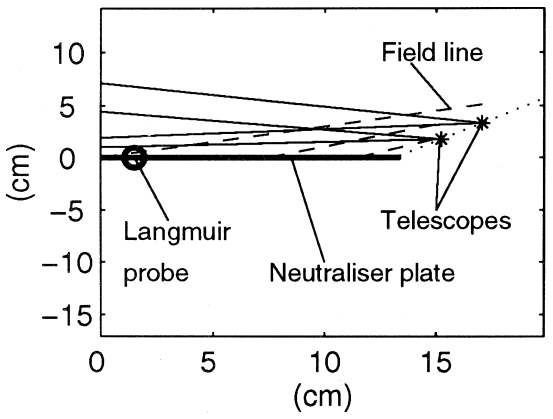

Fig. 1. Photograph and tangential view of the NP (vertical axis perpendicular to the figure).

3. ED current scan and Ne I, Ne II behaviour

To assess the effect of the depth of the perturbed region, an ED current (I_{ED}) scan has been performed, the depth being roughly proportional to I_{ED}. A series of discharges were performed at $I_p = 1.5$ MA, with an edge safety factor $q_\Psi = 2.8$. The minor radius was 0.74 m, and the major radius was 2.38 m. The volume average density $\langle n_e \rangle$ was 4.2×10^{19} m^{-3}, i.e. in the upper range of densities achievable in TS. The amount of neon injected in the discharge was between 0.007 and 0.02 Pa m^3 (depending on the pulse) and the duration of the puff was about 0.5 s. This value was chosen in order to have large enough Ne I and Ne II brightness on the spectrometer without modifying the radiated power by more than 0.1 MW (i.e. $\Delta P_{rad} \leqslant 20\%$). Due to the small amount of injected gas, no change in T_e or n_e on the neutraliser due to the neon puff was observed, except in one case. Therefore this series of pulses can be considered as a nonperturbative test of the ED effect on neon.

Two interlaced series of four pulses each have been selected, each constituting a full ED current scan (0, 20, 32 and 45 kA). In the first series, the spectrometer connected to the four in situ fibres was measuring the Ne I 585.2 nm line. In the second series the spectrometer was measuring the Ne II multiplet at 366.4–369.4–371.0 nm.

Fig. 2 shows the Ne I and Ne II brightness profiles corresponding to the four I_{ED} values, measured by the in situ fibres before neon is pumped out. Each profile is normalised to its maximum value. These brightness profiles have to be interpreted with care; in particular, due to the T_e-dependence of the rate coefficients relating the ion densities to the spectral line emissivities, they cannot be assumed to be strictly proportional to the Ne and Ne^+ density profiles. This is especially true for neutral neon, since the typical T_e (10–50 eV) measured on the NP corresponds to the greatest T_e-dependence of the neon ionisation and excitation rate coefficients. Also, as can be seen in Fig. 1, the lines of sight are not strictly parallel to the neutraliser plane, so they measure the integral of the emissivity on regions where T_e is not strictly uniform. Only a model taking into account the atomic data and the real geometry can deduce the

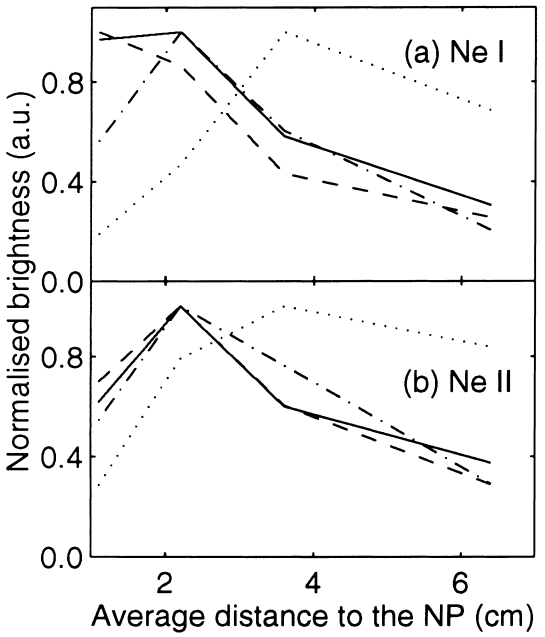

Fig. 2. Normalised brightness profiles of (a) Ne I 585.2 nm and (b) Ne II 369.4 nm. $I_{ED} = 0$ (solid line), 20 kA (dashed), 32 kA (dashed–dotted), 45 kA (dotted).

densities from the brightness profiles (see Section 5). However they give a qualitative idea on the neon behaviour in the ED configuration. Both for Ne I and Ne II a shift of the maximum brightness from the neutraliser surface toward the confined plasma can be seen. The radial profiles of the Ne IV (Fig. 3), V, VII and VIII line brightness (over the lower half of the plasma) are measured by a rotating mirror duochromator. An inward shift of the brightness peak can be seen together with a broadening of the brightness profiles on Ne IV and Ne V, indicating a T_e profile flattening [7]. The Ne VII brightness profile as measured by the duochromator is not modified by the ED perturbation (except at the maximum ED current value). This indicates that the perturbation is limited to a region where $T_e \leqslant 100$ eV. A rough estimate of the ratio $\rho_{e/c}$ of the edge neon density to the central neon density has been made using the Ne IV and Ne X brightness. To calculate $\rho_{e/c}$, the electron density in the region of Ne IV is assumed to behave either like the central density or like the density on the plate (the actual situation being probably inbetween). With both assumptions $\rho_{e/c}$ is found to increase by 40–50% when I_{ED} is increased from 0 to its maximum. It shows that despite the deeper penetration of the lower Ne ionisation stages the screening effect increases with the magnetic perturbation in these discharges.

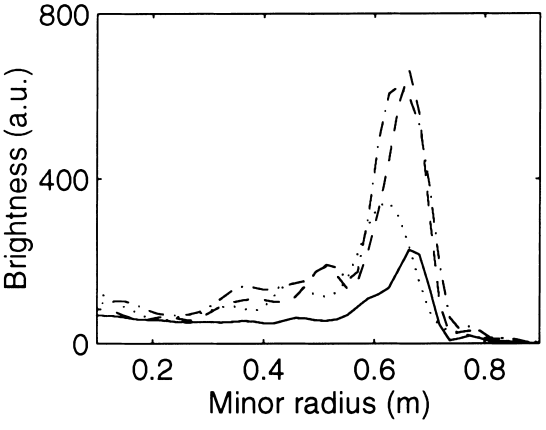

Fig. 3. Ne IV brightness profile as measured by the duochromator at $I_{ED} = 0$ (solid line), 20 kA (dashed), 32 kA (dashed–dotted), 45 kA (dotted).

4. Density scan and carbon behaviour

One of the interests of the ED configuration is to help in controlling the impurity penetration. However the ED effectiveness is closely related to the neutral production and ionisation length: as well for D as for intrinsic or injected impurities, they are functions of the density range in the NP area. In TS, three density regimes have been identified in the ED configuration [3], leading from a low recycling regime ($n_e^{edge} \propto \langle n_e \rangle$) at low volume average density up to a high recycling regime ($n_e^{edge} \propto \langle n_e \rangle^3$) and eventually to detachment (saturation then drop of n_e^{edge}) at the highest densities.

The experiment was performed at $I_p = 1.5$ MA, $q_\Psi = 2.75$. The minor radius was 0.74 cm, and the major radius was 2.38 m. The volume average density was increased during each pulse, the starting density being as close as possible to the largest density of the preceding pulse. To study the dependence of the brightness profiles on density we define two shape parameters: S_{12} the ratio of the signal from the line of sight closest to the plate to the signal from the second closest, and S_{23}, the ratio of the second to the third. A density scan over low and mid-range densities (1.5×10^{19}–3.6×10^{19} m^{-3}) was dedicated to the observation of C III 464.7 nm. Fig. 4 shows S_{12} for C III as a function of $\langle n_e \rangle$. The increase of S_{12} indicates that the C III maximum emissivity moves closer to the NP, in qualitative agreement with the expected reduction of the ionisation length. A second scan over a higher density range (3.2×10^{19}–4.8×10^{19} m^{-3}) was dedicated to observing Dα and the C II 658 nm multiplet. The Dα and C II brightness profiles at four different values of $\langle n_e \rangle$ are shown in Fig. 5. The Dα profile moves away from the NP as $\langle n_e \rangle$ is increased, while the C II profile changes in absolute value without detaching from the NP. At moderate density $S_{12} > 1$ and the brightness profiles are peaked close to the NP.

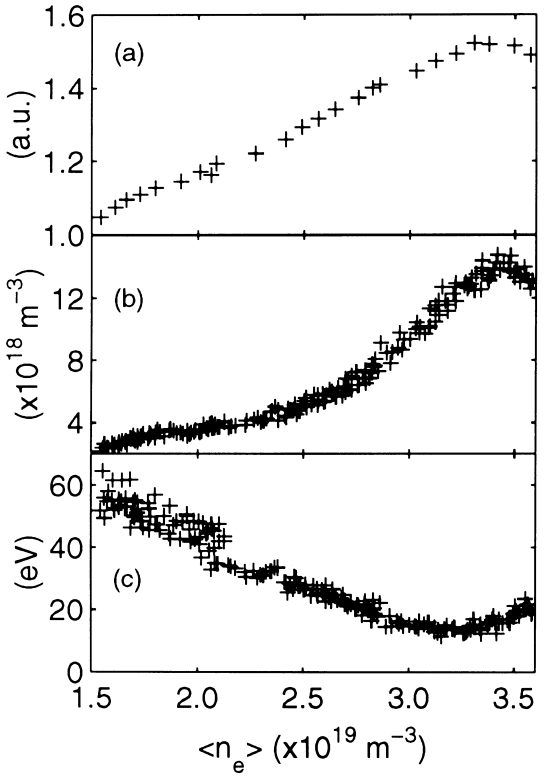

Fig. 4. Density ramp up: (a) C III shape parameter S_{12}; (b) n_e on the NP; (c) T_e on the NP.

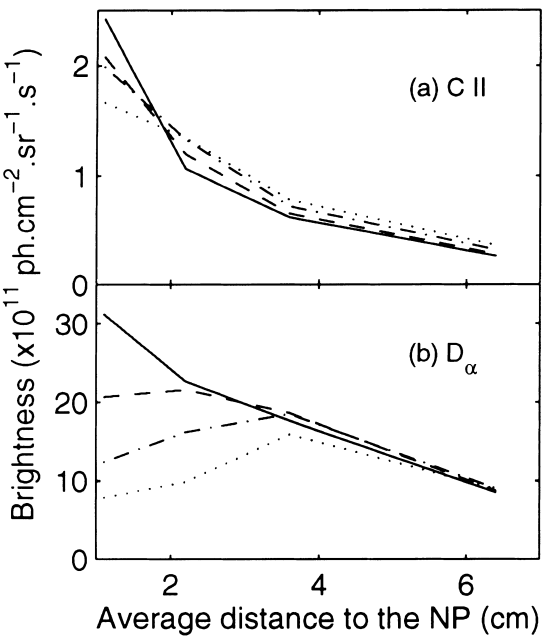

Fig. 5. Brightness profiles of (a) C II 658 nm and (b) Dα at $\langle n_e \rangle = 3.5 \times 10^{19}$ m^{-3} (solid line), 4.1×10^{19} m^{-3} (dashed), 4.5×10^{19} m^{-3} (dashed–dotted), 4.8×10^{19} m^{-3} (dotted).

The evolution of $S_{12}^{D\alpha}$, $S_{23}^{D\alpha}$ and n_e on the NP as a function of the volume average density is shown in Fig. 6. Note that $S_{12}^{D\alpha}$ drops below unity well before the Langmuir probe observes the transition from a high recycling regime to the detachment. The Langmuir probe detachment criterion (plateau of n_e^{edge}) is reached when S_{23} in turn drops below unity. On the contrary, because of the local density increase (6×10^{18}–10×10^{18} m^{-3}) and of the low ionisation potentials of the first two ionisation stages of carbon, the C II brightness profile does not detach. Also shown on Fig. 6 is the evolution of the ratio ρ_B of two bolometric chords viewing tangentially the plasma edge at a normalised radius of respectively 0.86 and 1. This ratio increases relatively smoothly during the transition from a high recycling regime to detachment. These observations suggest a continuous transition from attachment to detachment of the plasma (see also Ref. [8]).

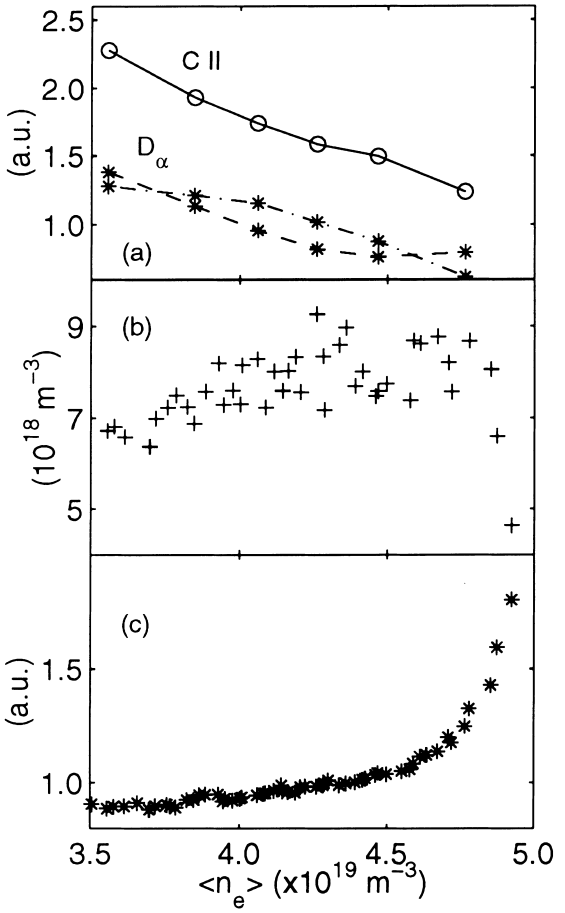

Fig. 6. (a) Shape parameters $S_{12}^{C\,II}$ (solid), $S_{12}^{D\alpha}$ (dashed) and $S_{23}^{D\alpha}$ (dashed–dotted); (b) electron density on the NP; (c) bolometry detachment parameter ρ_B (see text).

5. Modelling the impurity behaviour

To complete the data interpretation, modelling the various processes playing a role in the impurity behaviour is necessary, since no diagnostic gives direct access to the crucial quantities such as the impurity densities. Therefore a modelling effort has been made to extract these quantities from the data, both with the 2D model IMPEN [9], including only the main features of the problem (monoenergetic neutral velocity, n_e and T_e in the neutraliser area, simple description of the atomic physics processes), aimed at identifying the important parameters, and with the complete 3D Monte-Carlo code BBQ [10] describing in more detail the impurity production and recycling mechanisms along with the transport processes.

Radially away (up to 10–15 cm) from the NP no diagnostic gives direct access to either n_e or T_e. The usual assumption of an exponential decay at the edge is no longer valid in ED configuration. Therefore the parallel transport equations have been resolved. In the high recycling regime case, corresponding to most of the cases studied here, one finds that T_e increases linearly from the NP along a field line. The electron pressure is assumed to be constant along a field line, and the variation of n_e along a field line is deduced from that of T_e. In order to identify the main parameters playing a role in the impurity penetration, the 2D code IMPEN has been used to reproduce the optical fibre data. The direction of the field lines connected to the neutraliser is computed by the 3D code MASTOC [2] from the global magnetic parameters (I_p, B_T, q_ψ). The angle between the neutraliser plane and the connected field lines runs monotonously from about 8.5° near the Langmuir probe ('tip' of the NP) up to about 14° near the telescopes, the exact values depending on the magnetic parameters. The incident particle flux is assumed to be proportional to the sine of this angle. MASTOC results also show that, at maximum magnetic perturbation, one half of the NP is connected to the plasma. This is confirmed by the IR thermographic pictures for pulses with the same magnetic configuration as those considered in this paper. Therefore, we will assume that the neutral source (in relative units) increases monotonously from sin(8.5°) at the tip of the NP up to sin(12°) at the middle of the NP, then drops down to 0. For C II simulation the atomic data are taken from Ref. [11]. The C II brightness profiles have been simulated in three cases (Fig. 7) with increasing volume average density: (1) $\langle n_e \rangle = 3.5 \times 10^{19}$ m^{-3}, $n_e(\mathrm{NP}) = 9 \times 10^{18}$ m^{-3}, $T_e(\mathrm{NP}) = 40$ eV, (2) $\langle n_e \rangle = 4.4 \times 10^{19}$ m^{-3}, $n_e(\mathrm{NP}) = 10^{19}$ m^{-3}, $T_e(\mathrm{NP}) = 30$ eV, (3) $\langle n_e \rangle = 4.8 \times 10^{19}$ m^{-3}, $n_e(\mathrm{NP}) = 5 \times 10^{18}$ m^{-3}, $T_e(\mathrm{NP}) = 18$ eV. A neutral velocity of 5 eV has been found to fit the data in all cases. Assuming the electron pressure is uniform along a field line, the T_e parallel gradient is estimated to 5 eV cm^{-1} in the first case and 2 eV cm^{-1} in the second case. In the last case, however, the hypothesis of a uniform electron pressure along a field line leads to simulated profiles that do not fit the data. Uniform n_e and T_e give better results indicating that the plasma is not in the high recycling regime but rather approaching detachment. To go further in this study a more accurate description of the neutral production mechanisms is required.

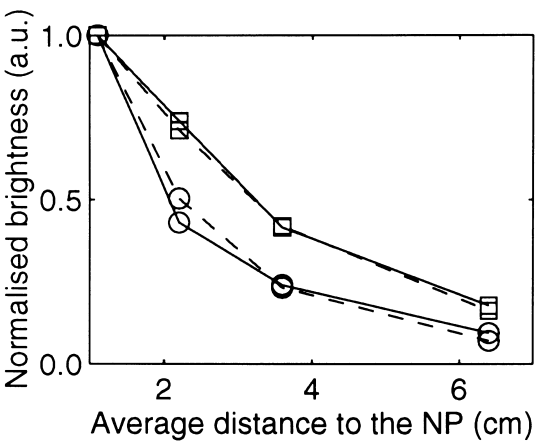

Fig. 7. Normalised C II profiles and IMPEN results. Solid line: experimental data; dashed: simulation. ○: case 1; □: case 2 (see text).

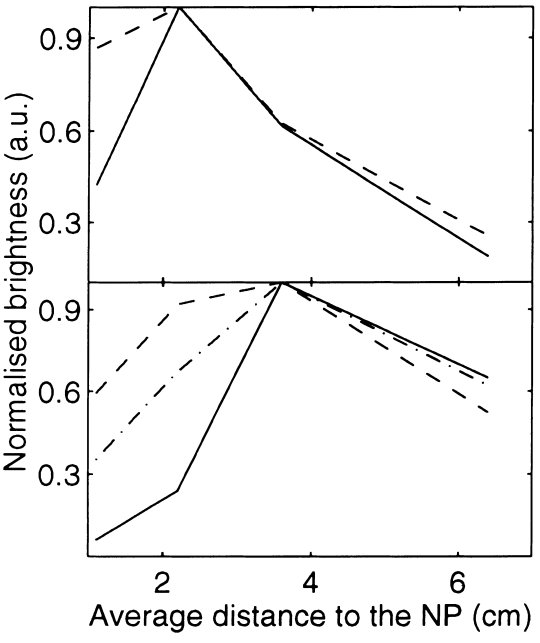

Fig. 8. Ne I experimental profiles and IMPEN results normalised to the maximum value. Top: $I_{ED} = 32$ kA; experimental data (solid line) and modelling (dashed); bottom: $I_{ED} = 45$ kA; experimental data (solid line), best fit (dashed) and best fit with $\langle \sigma v \rangle_{exc}$ shifted by 10 eV (dashed–dotted).

In the case of Ne I at $I_{ED} = 32$ kA and $I_{ED} = 45$ kA (Fig. 8), the trend in penetration is well reproduced using a neutral velocity of 1 eV. Assuming the incident neon particles are Ne^{2+} or Ne^{3+} and with an acceleration in the sheath of $Z(3T_e + 3T_i)$, an incidence angle of $37.5° \pm 2.5°$ is deduced from the energy backscattering coefficient tables calculated by the TRIM code [12]. The experimental brightness cannot be reproduced using in IMPEN an extended source along the NP. The source is more likely to be localised within a 3 cm area close to the Langmuir probe. Note that very few data [13,14] have been published on the Ne I $3p'[1/2]_0$ excitation rate coefficients. This is thought to be a major limitation to this study because the T_e range measured in these experiments is the region of greatest T_e-dependence of the ionisation and excitation rate coefficients.

The BBQ code has been used to compare the experimentally observed spectral line brightness with the recycling and penetration expected on the basis of models commonly in use. For the case of carbon penetration from the NP, generation in the form of physical sputtering of the carbon-coated B_4C plate by the incident D^+ ion flux is assumed. The sputtering rates are those described in Ref. [15]. The BBQ code selects the emitted C atom energy distribution from a Thomson distribution, which is a characteristic of physical sputtering. This leads to an emitted energy distribution with a high energy tail up to tens of eV for the conditions of these discharges. The trends in penetration depth are generally consistent between the code and the data.

For neon, the recycling is due to re-emission of the incident neon ion flux from the NP, and the dominant emission processes are reflection and thermal emission. The BBQ code employs the results of systematic TRIM code calculations [12] to calculate the energetic reflected distribution, taking the values for neon reflected from carbon for the impact energies of each case. Fig. 9 shows the BBQ results for Ne I distributions for the I_{ED} scan. The maximum value for each case is normalised to the maximum of the data for that shot. The BBQ calculations assume (as indicated by MASTOC calculations) that the neon ion influx spreads over an increasing neutraliser surface for increasing ED current. Fig. 10 shows, for n_e and T_e conditions of the case $I_{ED} = 20$ kA, the result of varying the assumed localisation of the incident neon ion flux. The area contributing to the neon flux was varied over the range indicated by MASTOC calculations for an increase in I_{DE} from 20 to 45 kA. With increasing wetted area (as I_{ED} increases) the decay length of the Ne I chordal profile calculated by BBQ is increased. Thus, the Ne I profile fit is sensitive to the detailed magnetic structure of the ED.

6. Conclusion

At high volume average density, penetration of the lower ionisation stages of neon increases with the ED magnetic perturbation essentially because of the T_e profile flattening, while the ratio of the edge neon density to the central neon density increases, even on the verge of detachment. The 2D code IMPEN indicates in this case rather uniform n_e and T_e profiles in the NP vicinity but both IMPEN and BBQ show the importance of an accurate incident flux description and of reliable atomic data.

At maximum magnetic perturbation and up to densities close to detachment the carbon penetration decreases. At high density, modelling the C II brightness profiles with IMPEN has been used to evaluate n_e and T_e in front of the NP. The best results are obtained with uniform electron pressure along field lines, with a

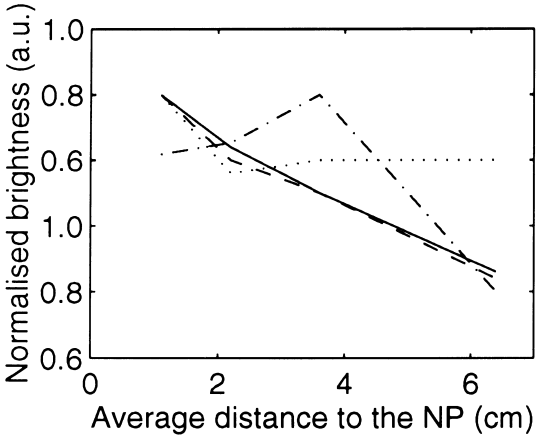

Fig. 9. BBQ results for Ne I brightness simulation. Same lines as Fig. 2.

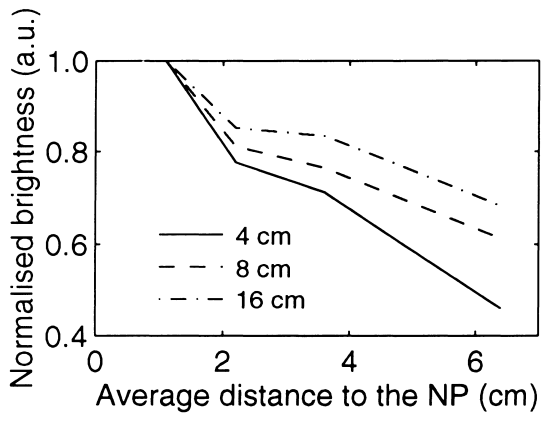

Fig. 10. Sensitivity of the Ne I brightness profile on the neon flux extension simulated with BBQ.

parallel T_e gradient decreasing when approaching detachment.

Basic trends are also reproduced with the BBQ code, with the same sensitivity to excitation rate coefficients, reflection energy and angle dependence and ED field configuration as with the IMPEN code.

References

[1] C. DeMichelis et al., Nucl. Fusion 35 (1995) 1133.
[2] Ph. Ghendrih, A. Grosman, H. Capes, Plasma Phys. Control. Fusion 38 (1996) 1653.
[3] B. Meslin et al., these Proceedings.
[4] W. Rowan et al., European Physical Society Conference on Controlled Fusion and Plasma Physics, vol. 11D, Madrid, 1987, p. 117.
[5] S. Takamura et al., Proceedings of the 13th IAEA International Conference on Plasma Physics and Controlled Fusion Research, vol. 1, Washington, 1990, p. 549.
[6] P. Monier-Garbet et al., Proceedings of the 14th IAEA International Conference on Plasma Physics and Controlled Fusion Research, vol. 1, Würzburg, 1992, p. 317.
[7] J. Payan et al., Nucl. Fusion 35 (1995) 1357.
[8] Ph. Ghendrih et al., these Proceedings.
[9] L. Chérigier et al., European Physical Society Conference on Controlled Fusion and Plasma Physics, vol. 21, Berchtesgaden, 1997, p. 201.
[10] J. Hogan et al., Proceedings of the 16th IAEA International Conference on Plasma Physics and Controlled Fusion Research, vol. 2, Montreal, 1996, p. 625.
[11] R. Phaneuf et al., ORNL-6090, 1987, Oak Ridge Nat. Lab.
[12] W. Eckstein, J. Nucl. Mater. 248 (1998) 1.
[13] D. Register et al., Phys. Rev. A 29 (1984) 1793.
[14] L. Machado et al., Phys. Rev. A 29 (1984) 1811.
[15] T. Ono et al., Sputtering yield formula for B_4C irradiated with monoenergetic ions at normal incidence, National Institute for Fusion Science, Japan, Report NIFS-DATA-34, April 1996.